Wakes in complex plasmas: A self-consistent kinetic theory

Roman Kompaneets,[1,*] Gregor E. Morfill,[1,2] and Alexei V. Ivlev[1]
[1]*Max-Planck-Institut für extraterrestrische Physik, Giessenbachstr. 1, 85748 Garching, Germany*
[2]*BMSTU Centre for Plasma Science and Technology, Moscow, 105005, Russia*
(Received 29 January 2016; published 1 June 2016)

In ground-based experiments with complex (dusty) plasmas, charged microparticles are levitated against gravity by an electric field, which also drives ion flow in the parent gas. Existing analytical approaches to describe the electrostatic interaction between microparticles in such conditions generally ignore the field and ion-neutral collisions, assuming free ion flow with a certain approximation for the ion velocity distribution function (usually a shifted Maxwellian). We provide a comprehensive analysis of our previously proposed self-consistent kinetic theory including the field, ion-neutral collisions, and the corresponding ion velocity distribution. We focus on various limiting cases and demonstrate how the interplay of these factors results in different forms of the shielding potential.

DOI: 10.1103/PhysRevE.93.063201

I. INTRODUCTON

A complex (or dusty) plasma is a plasma that contains charged dust microparticles [1–17]. Complex plasma experiments are generally performed with weakly ionized plasmas and microparticles of a few μm in diameter, which are charged negatively by collection of free electrons and ions from the plasma [2–6]. The equilibrium charges, typically of the order of -10^4e, are large enough to give rise to strong mutual electrostatic interaction between particles and, as a result, a plethora of self-organization phenomena. This allows us to use complex plasmas as a model system to study various processes in fluids and solids, by directly observing individual microparticles (see, e.g., studies of shock waves [18,19], crystallization and melting fronts [20], and dislocations in crystals [21]). In contrast to colloidal suspensions [22,23], which can be used for similar purposes, complex plasmas are characterized by weak damping and therefore enable investigations at the intrinsic dynamic time scales.

While there have been many studies of complex plasmas under microgravity conditions, most experiments are carried out on the ground. Usually they are performed in a radio-frequency discharge, where microparticles are levitated against gravity by the average electric field of the discharge [2,4] (although there have been experiments where the levivation was mainly due to the termophoretic force [24–26]). This electric field naturally arises to maintain the balance of the ion and electron currents on the electrodes; it increases toward the lower electrode (see, e.g., Fig. 7 or Ref. [27]), so microparticles find their equilibrium position at the height where the resulting electrostatic force on a particle is just enough to compensate for gravity (and the ion drag force [2,4], which is usually considerably smaller than the gravity force).

The electric field that levitates microparticles against gravity also drives ion flow in the parent neutral gas. Usually, the ion flow at the levitation position is more or less mobility limited, so its velocity can be estimated by equating the gravity force and the electrostatic force and using published data on mobility of ions in their parent gases [28]. Such estimates show that, depending on the pressure and particle size (mass), the flow velocity varies considerably from one experiment to another and can easily be smaller than, about the same as, and many times larger than the thermal velocity of neutrals.

The ion flow is a key factor determining the plasma shielding of, and hence the electrostatic interaction between, microparticles. It has long been known that the screening of the Coulomb potential in an anisotropic plasma is not exponential [29–31]. Moreover, an excess of positive charge is formed downstream of microparticles, which leads to nonreciprocal interaction forces between them [32–34]. Various theoretical models have been proposed to describe the interaction between microparticles in the presence of ion flow, predicting, in particular, the formation of an oscillatory wake structure downstream of the particle [35,36] and the possibility of attraction between particles in the plane perpendicular to the flow [37–39].

Existing analytical approaches to describe the shielding of microparticles generally ignore the presence of the field and ion-neutral collisions, assuming free ion flow with a certain approximation for the ion velocity distribution function, usually a shifted Maxwellian or, as a particular case, a shifted δ function (i.e., cold ion flow). However, there are three principal issues with such approaches:

(i) Measurements of ion velocity distributions in weakly ionized gas discharges show that in regions with considerable ion flow relative to the neutral gas, the distributions are generally far from being shifted Maxwellians [40]. The physical reason for this is quite obvious—ions collide with neutrals much more frequently than with each other, so the ion velocity distribution function cannot equilibrate.

(ii) The neglect of collisions is not justified for many experiments, because the ion-neutral collision length is often about or smaller than the characteristic interparticle distance.

(iii) It is not obvious when the electric field driving the flow can indeed be neglected in the analysis of the plasma perturbation due to a micropartile.

We have previously proposed a self-consistent kinetic theory to address these issues [41]. The model includes the electric field and ion-neutral collisions, and the unperturbed (by the microparticle) ion velocity distribution function is self-consistently calculated by considering the balance of the

*kompaneets@mpe.mpg.de

acceleration of ions in the field and collisions with neutrals. The field and collisions are included not only to calculate the unperturbed distribution but also are accounted for in the analysis of the plasma perturbation due to a microparticle. Of course, such an approach generally requires cumbersome calculations. We avoided this difficulty by considering the common case where the dominant mechanism of collisions is charge transfer, in which the ion and neutral simply exchange identities, and thus momenta [42,43]. Our further approximation was to assume the collision frequency to be velocity independent, which allowed for an elegant solution not only for the steady state but also for the ion susceptibility.

In reality, it is not the collision frequency but the cross section that is characterized by a weak (logarithmic) velocity dependence [43,44] (in the regime where charge transfer is the dominant mechanism of collisions). Nevertheless, the constant-collision-frequency model is a reasonable approximation to describe the particle shielding, as it yields velocity distributions qualitatively similar to those given by the constant-cross-section model [45,46]: Even in the strong-flow regime (i.e., where the flow velocity substantially exceeds the thermal velocity of neutrals), for both models the parallel-to-the-field velocity distribution very quickly reaches a maximum (at a velocity about the thermal velocity of neutrals) and then decays slowly (at velocities comparable to the flow velocity), which is also in accord with measurements [40]. In the strong-flow regime (which is the only limit where the shielding can be analytically calculated in the constant-cross-section model), we did not find any qualitative difference between the potentials given by the two models (see Sec. VII and Ref. [47]).

While we have previously used our constant-collision-frequency model for particular purposes, such as the calculation of the ion drag force [41] and investigation of the possibility of attraction between particles aligned perpendicular to the flow [47], in this paper we provide a comprehensive analysis, focusing on various limiting cases and demonstrating how the interplay of the field, collisions, and the non-Maxwellian form of the distribution function results in different forms of the shielding potential.

II. MODEL

We consider a microparticle of charge Q immersed in a weakly ionized plasma with ion flow. In our model, the ions are described by the kinetic equation,

$$\mathbf{v}\cdot\nabla f+\frac{e}{m}(\mathbf{E}_0-\nabla\varphi)\cdot\frac{\partial f}{\partial\mathbf{v}}=\mathrm{St}[f], \tag{1}$$

where $f(\mathbf{r},\mathbf{v})$ is the ion velocity distribution function, $\mathbf{E}_0$ is the electric field driving the ion flow, $\varphi(\mathbf{r})$ is the potential due to the microparticle, e is the elementary charge, and m is the ion mass (ions are assumed to be singly ionized). For the ion-neutral collision operator $\mathrm{St}[f]$, we use the Bhatnagar-Gross-Krook (BGK) form:

$$\mathrm{St}[f]=-\nu f(\mathbf{v})+\nu\Phi_M(v)\int f(\mathbf{v}')\,d\mathbf{v}', \tag{2}$$

where

$$\Phi_M(v)=\frac{1}{\left(2\pi v_T^2\right)^{3/2}}\exp\left(-\frac{v^2}{2v_T^2}\right) \tag{3}$$

is the normalized Maxwellian velocity distribution of neutrals, ν is the (velocity-independent) collision frequency, $v_T=\sqrt{T_n/m}$ is the thermal velocity of neutrals, and T_n is the neutral temperature. The BGK operator allows us to probe into the principal roles of the electric field and collisions. This operator *exactly* describes ion-neutral collisions under assumptions that (i) their dominant mechanism is charge transfer and (ii) the collision frequency is velocity independent. At room temperature, for argon (the gas most frequently used in complex plasma experiments), charge transfer is indeed the dominant mechanism when the flow velocity substantially exceeds the thermal velocity of neutrals; however, in this regime, charge transfer is characterized by a weak (logarithmic) velocity dependence of its cross section rather than the collision frequency [43,44]. In the opposite regime, where the flow velocity is less than the thermal velocity of neutrals, the dominant mechanism is polarization scattering [43], so the collision frequency is indeed velocity independent (as assumed), although the BGK operator does not precisely describe polarization scattering. Nevertheless, as we already pointed out in the Introduction, for large flow velocities (corresponding to the cold-neutral approximation), we have demonstrated that the BGK model and the constant-collision-length model yield similar results for the shielding of a microparticle (see Sec. VII and Ref. [47]).

Note that in Eq. (1), we have neglected the absorption of ions by the microparticle. This effect has received considerable attention in the case when the ion flow is absent [48–51]. However, in the regime of strong ion flow, the characteristic ion absorption cross section is considerably reduced [2], so the effect on the shielding potential is rather weak in this case (see Ref. [52] for a detailed discussion). It follows that stating from a certain (quite small) ion flow velocity, the ion absorption does not significantly modify the shielding potential. Formally, the absorption can be included in our model by using the approach of Refs. [48,53].

Concerning the electrons, we assume that they obey the Boltzmann distribution with a certain temperature T_e or, as a particular case, are just a homogeneous neutralizing background (which corresponds to the limit $T_e\to\infty$).

The model is closed by Poisson's equation,

$$\nabla\cdot\mathbf{E}_0-\nabla^2\varphi=\frac{e}{\varepsilon_0}\left[\int f\,d\mathbf{v}-n_e+Q\delta(\mathbf{r})\right], \tag{4}$$

where n_e is the electron density, ε_0 is the permittivity of free space, and the microparticle is treated as a point charge.

To solve Eqs. (1)–(4), we make two key assumptions.

(i) *Liner perturbation approximation.* We linearize Eqs. (1) and (4) with respect to the perturbations induced by the microparticle. This approximation is justified when the characteristic kinetic energy of ions is much larger than the potential energy $e\varphi$ at the distance equal to the characteristic screening length. This is usually the case for experiments in which the flow velocity significantly exceeds the thermal velocity of neutrals; even when the above energies are comparable (which is often the case for the remaining experiments),

our results should still provide a good representation of the wake structure, because the shielding becomes linear at large distances anyway.

(ii) *Homogeneous plasma approximation*. We assume that all unperturbed quantities are constant in space. Physically, this implies that the inhomogeneity scale is much larger than the distances characterizing the problem. Strictly speaking, this assumption requires $T_e \to \infty$, to ensure a homogeneous electron density profile. However, we will keep T_e finite to include the Boltzmann electron response into our model, i.e., while the unperturbed electron density is considered to be homogeneous, its response to the microparticle is taken to be $\delta n_e = n_e e\varphi/T_e$. To justify this assumption, we note that in experiments, microparticles can be levitated quite high in the presheath, where the inhomogeneity scale is considerably larger than the characteristic shielding length. Microparticles can also be levitated in the sheath, where the inhomogeneity is quite strong; for instance, for the well-known experiment of Ref. [54], where the interaction potential between microparticles was directly measured, the field inhomogeneity length at the levitation height was only twice as large as the observed screening length (see Ref. [55] for an analysis). However, we have recently demonstrated (in Ref. [56]) that even such a strong inhomogeneity does not affect the shielding potential significantly, unless very large distances from the microparticle are considered: We calculated the exact shielding potential of a point charge (in the collisionless Bohm sheath, using the linear-perturbation approximation) and found no considerable deviation from the potential obtained in the homogenous approximation, even when the point charge was located very deep in the sheath (see, e.g., Figs. 3 and 4 of Ref. [56]).

We find the homogeneous steady-state solution $f = f_0$ from Eqs. (1) and (4) by setting $\varphi = 0$ and $\partial f/\partial \mathbf{r} = \mathbf{0}$, i.e., the unperturbed velocity distribution is determined simply by the balance of the electric field and collisions, $(e\mathbf{E}_0/m)\cdot \partial f/\partial \mathbf{v} = \mathrm{St}[f]$. The resulting function $f_0(\mathbf{v})$ is not a shifted Maxwellian distribution. It can be written as

$$f_0(\mathbf{v}) = \frac{n_0}{\left(2\pi v_T^2\right)^{3/2}} \int_0^\infty \exp\left(-\xi - \frac{|\mathbf{v} - \xi \mathbf{v}_{\mathrm{fl}}|^2}{2v_T^2} \right) d\xi, \quad (5)$$

where n_0 is the unperturbed ion density and

$$\mathbf{v}_{\mathrm{fl}} = \frac{e\mathbf{E}_0}{m\nu} \quad (6)$$

is the flow velocity $(1/n_0)\int \mathbf{v} f_0\, d\mathbf{v}$. Equation (5) here is Eq. (3) of Ref. [41] but rewritten using another integration variable in order to show that $f_0(\mathbf{v})$ is an integral superposition of shifted Maxwellian distributions with exponential weights. The longitudinal velocity distribution $f_{0,z}(v_z)$ is plotted in Fig. 1. The difference from a shifted Maxwellian distribution becomes especially evident at large v_{fl}/v_T, when the solution (5) becomes highly asymmetric with respect to the position of its maximum. This can also be illustrated by considering the limit of cold neutrals, $v_T \to 0$. Equation (5) becomes

$$f_0(\mathbf{v}) = \frac{n_0}{v_{\mathrm{fl}}} \exp\left(-\frac{v_z}{v_{\mathrm{fl}}} \right) \delta(v_x)\delta(v_y), \quad v_z > 0,$$
$$f_0(\mathbf{v}) = 0, \quad v_z < 0, \quad (7)$$

where δ denotes the δ function and the z axis is in the direction of $\mathbf{E}_0$.

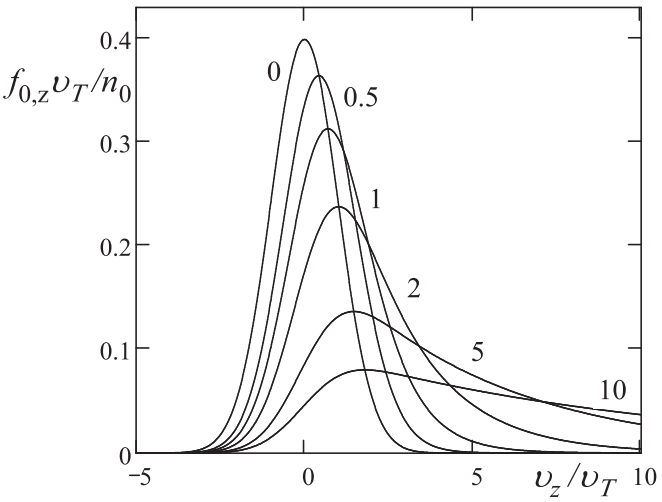

FIG. 1. Steady-state solution. Shown is the longitudinal velocity distribution $f_{0,z} = \int_{-\infty}^{\infty}\int_{-\infty}^{\infty} f_0\, dv_x\, dv_y$, where the z axis is in the direction of the field. Different lines correspond to different strengths of the field, measured in terms of the parameter v_{fl}/v_T (marked by numbers).

We have analyzed the stability of this steady state with respect to ion perturbations (see Ref. [57] for detailed investigation). For $T_e \to \infty$, the stability region is approximately described by $v_{\mathrm{fl}}/v_T \gtrsim 8$ and $\nu/\omega_p \lesssim 0.3$, where $\omega_p = [n_0 e^2/(\varepsilon_0 m)]^{1/2}$ is the ion plasma frequency. A finite T_e results in the increase of the above threshold on velocity and decrease of the threshold on the collision frequency. Our linear analysis, reported below, is physically meaningful only inside this stability domain. Note that most experiments fall within that domain, although some are near its boundary.

The resulting particle potential is [41]

$$\varphi(\mathbf{r}) = \frac{Q}{4\pi\varepsilon_0 r} + \frac{Q}{8\pi^3\varepsilon_0} \int \frac{\exp(i\mathbf{k}\cdot\mathbf{r})}{k^2} \left(\frac{1}{D(\mathbf{k})} - 1 \right) d\mathbf{k}, \quad (8)$$

and the static dielectric function $D(\mathbf{k})$ is given by

$$D(\mathbf{k}) = 1 + \frac{n_0 e^2}{\varepsilon_0 m \nu^2} \frac{B(\mathbf{k})}{1 - A(\mathbf{k})}, \quad (9)$$

where

$$A(\mathbf{k}) = \int_0^\infty \exp[-\Psi(\mathbf{k},\eta)]\, d\eta \quad (10)$$

and

$$B(\mathbf{k}) = \int_0^\infty \frac{\eta \exp[-\Psi(\mathbf{k},\eta)]}{1 + ik_z v_{\mathrm{fl}}\eta/\nu}\, d\eta \quad (11)$$

are defined via the function $\Psi(\mathbf{k},\eta)$ given by

$$\Psi(\mathbf{k},\eta) = \eta + \frac{1}{2}\left[\frac{ik_z v_{\mathrm{fl}}}{\nu} + \left(\frac{|\mathbf{k}| v_T}{\nu} \right)^2 \right] \eta^2. \quad (12)$$

We use the following transformation to normalize quantities:

$$\frac{\varphi}{Q/(4\pi\varepsilon_0\lambda)} \to \varphi, \quad \frac{\nu}{\omega_p} \to \nu,$$
$$\frac{\mathbf{v}_{\mathrm{fl}}}{v_T} \to \mathbf{v}_{\mathrm{fl}}, \quad \frac{\mathbf{r}}{\lambda} \to \mathbf{r}, \quad (13)$$

where

$$\lambda = \frac{v_T}{\omega_p} \tag{14}$$

is a characteristic length. (In the absence of the flow, λ becomes the ion Debye length; for finite E_0, the ion Debye length is not defined because of the non-Maxwellian form of the velocity distribution.) We also introduce the neutral-to-electron temperature ratio,

$$\tau = \frac{T_n}{T_e}. \tag{15}$$

In our analysis below, we mainly focus on limiting cases in which the potential can be calculated analytically. The calculations are highly tedious but conceptually straightforward, as they are mainly based on expansion of an integrand in a series of a small parameter and subsequently integrating the required number of terms of the series. We omit the derivations and point out that the analytical results presented below have been verified by comparing them with direct numerical calculations of the exact potential (8).

III. WEAKLY COLLISIONAL LIMIT

Let us first consider the limit of infinitely small E_0 and ν but a finite ratio of these, i.e., a finite $v_{\rm fl}$. Physically, this corresponds to free ion flow (in the absence of field and collisions) with the unperturbed velocity distribution of the non-Maxwellian form described by Eq. (5). Considering this limit allows us to address specifically the role of the non-Maxwellian shape of the distribution.

At large distances, the potential has an r^{-3} dependence,

$$\varphi(\mathbf{r}) = \frac{F(\theta)}{r^3} + o(r^{-3}), \tag{16}$$

where

$$F(\theta) = -\frac{i}{\pi^2} \lim_{\eta\to+0} \int_{-1}^{1} d\mu \int_0^{2\pi} \times \frac{d\alpha}{G(\mu\cos\theta - \sqrt{1-\mu^2}\sin\theta\cos\alpha)(\mu+i\eta)^3}, \tag{17}$$

$$G(x) = \tau + \int_0^\infty \frac{t\exp(-t^2/2)}{1+ix v_{\rm fl} t}\, dt, \tag{18}$$

and θ is the angle between $\mathbf{r}$ and the flow direction. In the plane perpendicular to the flow ($\theta = \pi/2$), the potential at large distances can be simplified,

$$\varphi(r,\pi/2) = \frac{v_{\rm fl}}{2\pi r^3} \frac{\partial}{\partial v_{\rm fl}} \int_0^{2\pi} \frac{d\alpha}{G(\cos\alpha)} + o(r^{-3}). \tag{19}$$

Figure 2 shows the coefficient of the r^{-3} dependence in Eq. (19) as a function of $v_{\rm fl}$ and τ. This coefficient remains positive for all $v_{\rm fl}$ and τ, meaning that the long-range electrostatic interaction forces between microparticles are always repulsive.

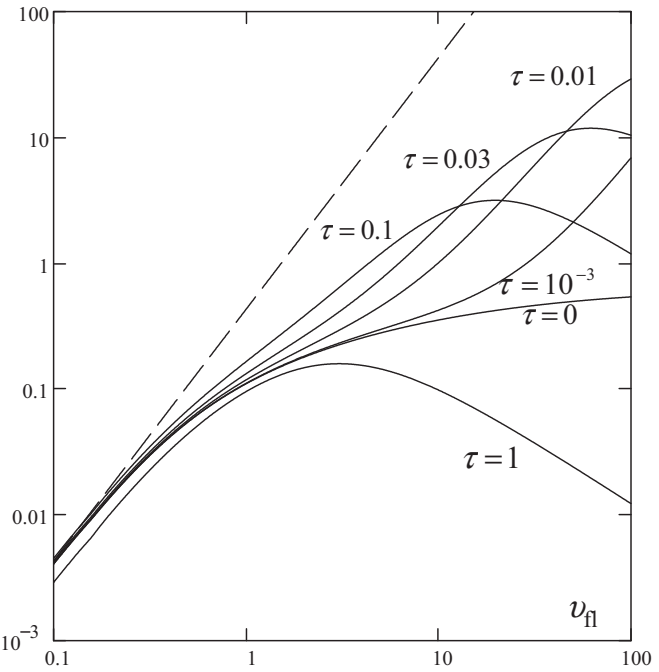

FIG. 2. The $1/r^3$ coefficient in Eq. (19) determining the potential at large distances in the plane perpendicular to the flow in the weakly collisional limit. The coefficient is plotted as a function of $v_{\rm fl}$ for several values of τ. The dashed line shows the $\propto v_{\rm fl}^2$ behavior at small velocities and $\tau = 0$, see Eq. (20) for $\theta = \pi/2$.

A simple explicit expression for the potential can be obtained in the limit of small $v_{\rm fl}$ and large r:

$$\varphi(\mathbf{r}) = \frac{\exp(-r\sqrt{1+\tau})}{r} - \sqrt{\frac{8}{\pi}} \frac{v_{\rm fl}\cos\theta}{(1+\tau)^2 r^3} + 2\left[1 - \frac{\pi}{4(1+\tau)}\right] \frac{v_{\rm fl}^2(1-3\cos^2\theta)}{(1+\tau)^2 r^3} + o\left[\frac{\exp(-r\sqrt{1+\tau})}{r}\right] + o\left(\frac{v_{\rm fl}^2}{r^3}\right). \tag{20}$$

(It does not matter which limit is taken first, $v_{\rm fl} \to 0$ or $r \to \infty$; however, it is essential that these limits are taken *after* the limit $\nu \to 0$). The dominant term in Eq. (20) is dipolelike: It has the same angular dependence as a bare dipole potential, $\propto \cos\theta$, although the radial dependence is r^{-3}, which differs from the r^{-2} dependence of the bare dipole potential. In the plane perpendicular to the flow, this term vanishes, so the next, quadrupole-like, term comes into play. The latter is always positive in that plane, which means repulsive interactions between microparticles aligned perpendicularly to the flow.

Interestingly, if we replace the BGK velocity distribution (5) by a shifted Maxwellian with the same flow velocity, and set $\tau = 0$ for simplicity, then the resulting potential (in the limit of small $v_{\rm fl}$ and large r) becomes

$$\varphi(\mathbf{r}) = \frac{\exp(-r)}{r} - \sqrt{\frac{8}{\pi}} v_{\rm fl}\cos\theta - \left(\frac{\pi}{2} - 1\right) \frac{v_{\rm fl}^2(1-3\cos^2\theta)}{r^3} + o\left[\frac{\exp(-r)}{r}\right] + o\left(\frac{v_{\rm fl}^2}{r^3}\right). \tag{21}$$

While the first-order expansion term ($\propto v_{fl}$) in Eq. (21) coincides with its counterpart in Eq. (20), there is an important difference between the second-order terms: For a shifted Maxwellian, two particles aligned perpendicularly to the flow attract each other at large distances. The difference in the second-order terms is obviously due to the difference in the distribution functions. This highlights the importance of the shape of the velocity distribution function even for small flow velocities.

Furthermore, our direct numerical calculations of the potential for finite v_{fl} and r (in the limit $\nu \to 0$) show that only one potential minimum is formed in the wake downstream of the particle. This is in contrast to the case of a shifted Maxwellian, where a series of potential minima can be formed, depending on the flow-to-thermal velocity ratio and the electron-to-ion temperature ratio [36,58].

IV. SMALL FLOW VELOCITIES

Let us now consider the case of a finite collision frequency and small electric field (i.e., a finite ν and small v_{fl}). Expanding the potential in a series of v_{fl}, we obtain

$$\varphi(\mathbf{r}) = \varphi_0(r) + v_{fl}\varphi_1(r)\cos\theta + v_{fl}^2\varphi_2(r)\cos^2\theta + v_{fl}^2\varphi_3(r)\sin^2\theta + o\left(v_{fl}^2\right), \tag{22}$$

where

$$\varphi_0(r) = \frac{\exp(-r\sqrt{1+\tau})}{r} \tag{23}$$

and the functions $\varphi_{1,2,3}(r)$ are given in Appendix. At large r, these functions have the following asymptotic expressions:

$$\varphi_1(r) = -\frac{\nu}{r^2(1+\tau)^2} + o(r^{-2}), \tag{24}$$

$$\varphi_2(r) = -\frac{2(\nu^2 - 2 - 2\tau\nu^2 + 2\tau^2)}{r^3(1+\tau)^4} + o(r^{-3}), \tag{25}$$

$$\varphi_3(r) = \frac{\tau\nu^2}{2r(1+\tau)^3} - \frac{1}{2}\varphi_2(r) + o(r^{-3}). \tag{26}$$

Four important observations can be made about these expressions, as discussed below:

(i) The asymptotic behavior of the potentials (22) and (20) at large distances do not match in the limit $\nu \to 0$. This is an expected effect: To derive the potential (20), we took the limit $\nu \to 0$ *before* $r \to \infty$, thereby restricting our analysis to distances smaller than the ion-neutral collision length. In contrast, Eq. (22) together with Eqs. (24)–(26) describes the true asymptptic behavior at large distances as the parameter ν is considered to be finite. Thus, at small but finite ν the potential first reaches the "collisionless" asymptote described by Eq. (20) and only thereafter, when r becomes larger than the ion-neutral collision length, does it tend to the asymptotic form of Eqs. (24)–(26). This is illustrated in Fig. 3, where we show the function $\varphi_3(r)$ for a small ν.

(ii) The asymptotic expression for the function $\varphi_1(r)$ is exactly a bare dipole potential, with the dipole moment $\nu v_{fl}(1+\tau)^{-2}$.

(iii) At large distances, the dominant contribution to $\varphi(\mathbf{r})$ is the r^{-1} term in $\varphi_3(r)$. That term is proportional to τ, which is of the order 10^{-2} in experiments, so that term generally plays a role only at very large distances. It exactly vanishes on the z axis.

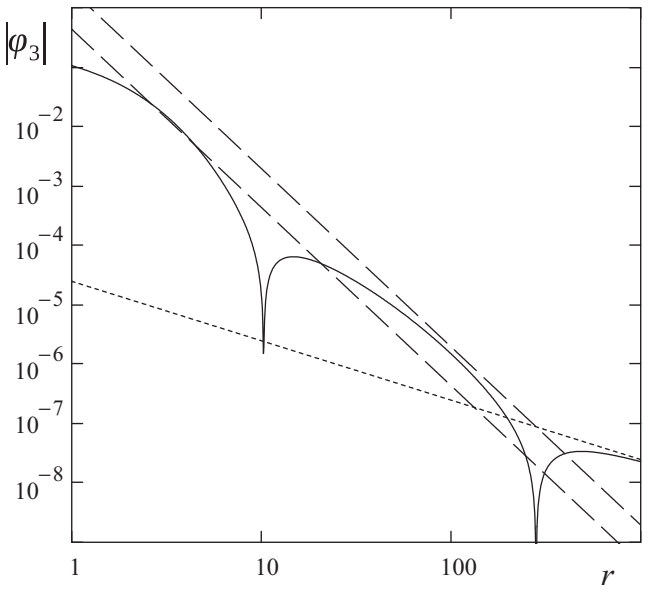

FIG. 3. The absolute value of the function $\varphi_3(r)$, characterizing the potential in the plane perpendicular to the flow. The solid line shows $|\varphi_3(r)|$ itself, plotted for $\zeta = 0.1$ and $\tau = 5 \times 10^{-3}$. The two dashed lines indicate the following r^{-3} asymptotes: The upper line is the second term in Eq. (26), and the lower line is the third term in Eq. (20) (for $\theta = \pi/2$). The dotted line is the r^{-1} asymptote described by the first term in Eq. (26). (While in experiments distances $r \sim 10^3\lambda$ are irrelevant, this calculation merely illustrates how the asymptotic laws work together; for other parameter values, the r^{-1} term can come into play at smaller distances and suppress the distance ranges where the r^{-3} asymptotes are a good approximation).

(iv) In $\varphi_3(r)$, which describes the asymptotic behavior in the plane perpendicular to the flow ($\theta = \pi/2$), the term $-\varphi_2(r)$ is attractive for $\nu < \sqrt{2}$ (assuming $\tau \ll 1$, as in experiments). In this case, $\varphi(r,\pi/2)$ first reaches a minimum and then, when the Coulomb-like term comes into play, again becomes positive, reaching a maximum and then slowly decaying to zero.

V. LARGE FLOW VELOCITIES

Let us now consider the limit of very large flow velocities (i.e., large v_{fl} and finite ν). Perhaps the most convenient way to do this mathematically is to take the limit of cold neutrals, $v_T \to 0$. To do so, we use the flow velocity v_{fl} instead of v_T to normalize φ and r, i.e., instead of λ we employ

$$\lambda_{fl} = \frac{v_{fl}}{\omega_p}. \tag{27}$$

In this limit of cold neutrals, the potential can be written in a relatively simple form for $T_e \to \infty$ as

$$\varphi(\mathbf{r}) = \frac{2}{\pi}\mathrm{Re}\int_0^\infty \frac{K_0(k_z r\sin\theta)}{H(k_z)}\exp(ik_z r\cos\theta)\,dk_z, \tag{28}$$

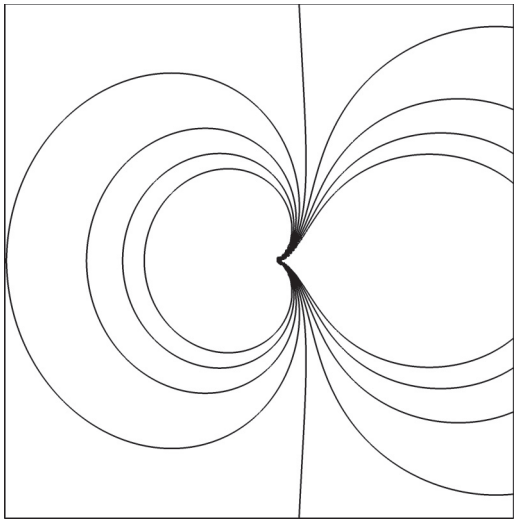

FIG. 4. A contour plot of the potential in the cold-neutral approximation for $\nu = 0.3$. The dimensions are $4\lambda_{\rm fl} \times 4\lambda_{\rm fl}$, the charge is in the center, and the flow is to the right.

where

$$H(k_z) = 1 + \frac{\int_0^\infty t \exp(-t\nu - ik_z \nu t^2/2)(1 + ik_z t)^{-1}\, dt}{1 - \nu \int_0^\infty \exp(-t\nu - ik_z \nu t^2/2)\, dt} \tag{29}$$

and K_0 is the zero-order modified Bessel function of the second kind. [Here, compared to Eq. (8), the integration variable k_z is normalized by $\lambda_{\rm fl}^{-1}$.]

At large distances, the potential (28) is simplified to

$$\varphi(\mathbf{r}) = -\frac{\nu \cos\theta}{r^2} + \frac{\nu^2 - 2}{r^3}(1 - 3\cos^2\theta) + o(r^{-3}). \tag{30}$$

Interestingly, written in the dimensional form, the asymptotic potential (30) exactly coincides with the asymptotic potential for $v_{\rm fl} \ll 1$ (for $\tau = 0$), given by Eqs. (22)–(26), i.e., we have the same dipole term and, for $\nu < \sqrt{2}$, the possibility of attraction between particles aligned perpendicular to the flow.

While the long-distance behavior of the potential at large flow velocities is similar to the low-velocity case, there are some important differences at shorter distances. By numerically analyzing the potential (28), we have found that it experiences oscillations downstream of the particle and that it diverges logarithmically for $\theta = 0$, both features being absent for the low-velocity case. The divergence is due to the cold-neutral approximation, i.e., it disappears for finite T_n. A contour plot of the potential (28) is shown in Fig. 4. (To see the oscillations, calculations must be performed for distances considerably larger than the dimensions of the contour plot shown in Fig. 4).

Another difference from the low-velocity case, found numerically for finite T_e, is that the potential decays exponentially with the distance in the plane perpendicular to the flow.

VI. GENERAL CASE

By numerically analyzing the potential in the general case, we have found that there is a smooth transition between all the limiting cases considered above, so the dependence of the shielding potential on $v_{\rm fl}$, ν, and τ can be qualitatively understood by considering the above limits. To illustrate the behavior at finite $v_{\rm fl}$, ν, and τ, we have chosen parameter values of the experiment of Ref. [54] and plotted the resulting potential in Fig. 5.

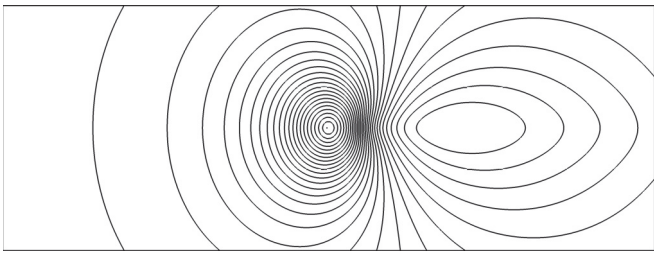

FIG. 5. The contour plot of the potential for $v_{\rm fl} = 8$, $\nu = 0.3$, and $\tau = 10^{-2}$. The dimensions are $30\lambda \times 10\lambda$ (or $3.75\lambda_{\rm fl} \times 1.25\lambda_{\rm fl}$), the charge is in the center, and the flow is to the right.

VII. ON THE RELIABILITY OF THE BGK APPROXIMATION

Let us now address the reliability of the BGK approximation. As explained above, ion-neutral collisions in the regime of strong ion flow are better described by the constant-cross-section approximation:

$$\mathrm{St}[f] = \int \frac{|\mathbf{v}' - \mathbf{v}|}{\ell}[\Phi_M(v) f(\mathbf{v}') - \Phi_M(v') f(\mathbf{v})] d\mathbf{v}', \tag{31}$$

where ℓ is the collision length. In the limit of cold neutrals, the operator (31) simplifies to

$$\mathrm{St}[f] = -\frac{v f(\mathbf{v})}{\ell} + \frac{\delta(\mathbf{v})}{\ell} \int f(\mathbf{v}') v'\, d\mathbf{v}' \tag{32}$$

(allowing semianalytical calculation of the shielding potential). The resulting steady-state velocity distribution is

$$f_0(\mathbf{v}) = \frac{2n_0}{\pi v_{{\rm fl},\ell}} \exp\left(-\frac{v_z^2}{\pi v_{{\rm fl},\ell}^2}\right)\delta(v_x)\delta(v_y), \quad v_z > 0,$$
$$f_0(\mathbf{v}) = 0, \quad v_z < 0, \tag{33}$$

where $v_{{\rm fl},\ell} = |\int \mathbf{v} f_0\, d\mathbf{v}|/n_0 = \sqrt{2eE_0\ell/(\pi m)}$ is the flow velocity in the constant cross-section case. Comparing Eq. (33) with Eq. (7), we note that these distributions are similar in that they both describe a smooth monotonic "decay" characterized by the respective flow velocity. Clearly, the tail of the distribution (i.e., $v \gg v_{\rm fl}, v_{{\rm fl},\ell}$) does not play any role in the particle shielding (because of the small number and high energies of the ions in that tail); for the bulk of the distribution (i.e., $v \sim v_{\rm fl}, v_{{\rm fl},\ell}$), which determines the shielding, there is only a moderate quantitative (but not qualitative) difference between the behaviors of the two distribution function.

It is therefore not an unexpected finding that the particle potential $\varphi_\ell(\mathbf{r})$ in the constant-cross-section model (in the cold-neutral approximation) at large distances is qualitatively similar to its counterpart for the BGK model. By solving the kinetic equation (1) with the collision operator (31), we have derived the following expression for the potential at large

distances for $T_e \to \infty$:

$$\varphi_\ell(\mathbf{r}) = -\frac{2\sqrt{2}\cos\theta}{r^2\ell(1+\cos^2\theta)^{3/2}} + \frac{\sqrt{2}J(\theta,\ell)}{12r^3(1+\cos^2\theta)^{7/2}} + o(r^{-3}), \quad (34)$$

where

$$J(\theta,\ell) = 60\ell^{-2} - 1 - (456\ell^{-2}+86)\cos^2\theta + (204\ell^{-2}+215)\cos^4\theta, \quad (35)$$

r and ℓ are normalized by the characteristic length $\lambda_\ell = [\varepsilon_0 E_0 \ell/(n_0 e)]^{1/2}$, and φ_ℓ is normalized by $Q/(4\pi\varepsilon_0\lambda_\ell)$. In particular, the potential (34) has a dipolelike contribution (i.e., the first term), which is merely corrected by a factor $(1+\cos^2\theta)^{-3/2}$. Also, similarly to the BGK case, the term following the dipolelike contribution is attractive when the collision length is large enough. At finite distances, we found numerically no qualitative difference between the particle potentials given by the two models.

In the general case of a finite thermal velocity of neutrals, the steady-state velocity distribution in the constant cross-section case has been analyzed in Refs. [45,46]. In particular, it has been pointed out that, regardless of the ratio between the flow velocity and the thermal velocity of neutrals, the BGK model is a very good approximation to describe the distribution function in the v_z range from negative velocities to the location of its maximum. The physical reason for this is quite obvious: As the maximum is always located at $v_z \sim v_T$, the probability for an ion from the above velocity range to encounter a collision with a neutral per unit time does not strongly depend on the velocity of the ion (as neutrals move with comparable velocities).

We conclude that the BGK collision integral is indeed an excellent model to probe into the principal effect of the field and collisions on the particle shielding.

VIII. CONCLUSIONS

We have analyzed a self-consistent kinetic model that includes the electric field driving the flow, ion-neutral collisions, and the non-Maxwellian velocity distribution of ions and explained how the interplay of these factors results in different forms of the shielding potential. Our main conclusion is that it is generally essential to account for the above factors, to ensure that the results are at least qualitatively reliable. In particular, taking into account the non-Maxwellian form of the distribution function in the weakly collisional regime results in the disappearance of both the oscillatory wake structure and attraction between microparticles aligned perpendicular to the flow—effects predicted by the model with a shifted Maxwellian distribution. However, a finite field and collision frequency can again give rise to the above effects, in addition to the collisional dipole contribution and a $1/r$ asymptotic behavior at large distances in the plane perpendicular to the flow. Overall, the form of the shielding potential varies considerably across parameter regimes, and our work, focused on various limiting cases, provides a basic guide as to how changing parameters affects the interaction between microparticles.

ACKNOWLEDGMENTS

The work received funding from the European Research Council under the European Union's Seventh Framework Programme, ERC Grant No. 267499.

APPENDIX: EXPRESSIONS FOR $\varphi_{1,2,3}(r)$

The functions $\varphi_{1,2,3}(r)$ are given by

$$\varphi_1(r) = -\frac{2}{\pi r^2}\int_0^\infty \frac{kr\cos kr - \sin kr}{(k^2+1+\tau)^2} g_1(\nu/k)\,dk, \quad (A1)$$

$$\varphi_2(r) = -\frac{2}{\pi r^3}\int_0^\infty \frac{2kr\cos kr + (k^2r^2-2)\sin kr}{k(k^2+1+\tau)^3} \times \left[g_2(\nu/k)(k^2+1+\tau) + g_1^2(\nu/k)\right] dk, \quad (A2)$$

and

$$\varphi_3(r) = \frac{2}{\pi r^3}\int_0^\infty \frac{kr\cos kr - \sin kr}{k(k^2+1+\tau)^3} \times \left[g_2(\nu/k)(k^2+1+\tau) + g_1^2(\nu/k)\right] dk. \quad (A3)$$

They are expressed via two auxillary functions,

$$g_1(x) = \frac{\mathrm{erfcx}(x/\sqrt{2})}{-\sqrt{2/\pi} + x\,\mathrm{erfcx}(x/\sqrt{2})} \quad (A4)$$

and

$$g_2(x) = \frac{\sqrt{2\pi}\,x(7-x^2)\mathrm{erfcx}(x/\sqrt{2}) - 4\pi x^2\,\mathrm{erfcx}^2(x/\sqrt{2}) + 2x^2 - 8}{[2-\sqrt{2\pi}\,x\,\mathrm{erfcx}(x/\sqrt{2})]^2}, \quad (A5)$$

where

$$\mathrm{erfcx}(x) = \frac{2}{\sqrt{\pi}}\exp(x^2)\int_x^\infty \exp(-t^2)\,dt, \quad (A6)$$

is the scaled complementary error function. At large r, Eqs. (A1)–(A3) are reduced to Eqs. (24)–(26).

[1] V. E. Fortov and G. E. Morfill, *Complex and Dusty Plasmas* (CRC Press, London, 2010).
[2] V. E. Fortov, A. V. Ivlev, S. A. Khrapak, A. G. Khrapak, and G. E. Morfill, Phys. Rep. **421**, 1 (2005).
[3] O. Ishihara, J. Phys. D: Appl. Phys. **40**, R121 (2007).
[4] G. E. Morfill and A. V. Ivlev, Rev. Mod. Phys. **81**, 1353 (2009).
[5] P. K. Shukla and B. Eliasson, Rev. Mod. Phys. **81**, 25 (2009).
[6] M. Bonitz, C. Henning, and D. Block, Rept. Prog. Phys. **73**, 066501 (2010).

[7] S. A. Khrapak, B. A. Klumov, P. Huber, V. I. Molotkov, A. M. Lipaev, V. N. Naumkin, A. V. Ivlev, H. M. Thomas, M. Schwabe, G. E. Morfill *et al.*, Phys. Rev. E **85**, 066407 (2012).

[8] S. A. Khrapak, M. H. Thoma, M. Chaudhuri, G. E. Morfill, A. V. Zobnin, A. D. Usachev, O. F. Petrov, and V. E. Fortov, Phys. Rev. E **87**, 063109 (2013).

[9] M. Schwabe, S. Zhdanov, C. Räth, D. B. Graves, H. M. Thomas, and G. E. Morfill, Phys. Rev. Lett. **112**, 115002 (2014).

[10] A. V. Ivlev, S. K. Zhdanov, M. Lampe, and G. E. Morfill, Phys. Rev. Lett. **113**, 135002 (2014).

[11] P. Hartmann, A. Z. Kovács, A. M. Douglass, J. C. Reyes, L. S. Matthews, and T. W. Hyde, Phys. Rev. Lett. **113**, 025002 (2014).

[12] I. Laut, S. K. Zhdanov, C. Räth, H. M. Thomas, and G. E. Morfill, Phys. Rev. E **93**, 013204 (2016).

[13] B. J. Harris, L. S. Matthews, and T. W. Hyde, Phys. Rev. E **91**, 063105 (2015).

[14] H. Thomsen and M. Bonitz, Phys. Rev. E **91**, 043104 (2015).

[15] S. A. Khrapak and H. M. Thomas, Phys. Rev. E **91**, 033110 (2015).

[16] L. Couëdel, S. Zhdanov, V. Nosenko, A. V. Ivlev, H. M. Thomas, and G. E. Morfill, Phys. Rev. E **89**, 053108 (2014).

[17] P. Hartmann, Z. Donkó, M. Rosenberg, and G. J. Kalman, Phys. Rev. E **89**, 043102 (2014).

[18] Y. Nakamura, H. Bailung, and P. K. Shukla, Phys. Rev. Lett. **83**, 1602 (1999).

[19] D. Samsonov, S. K. Zhdanov, R. A. Quinn, S. I. Popel, and G. E. Morfill, Phys. Rev. Lett. **92**, 255004 (2004).

[20] M. Rubin-Zuzic, G. E. Morfill, A. V. Ivlev, R. Pompl, B. A. Klumov, W. Bunk, H. M. Thomas, H. Rothermel, O. Havnes, and A. Fouquét, Nat. Phys. **2**, 181 (2006).

[21] V. Nosenko, G. E. Morfill, and P. Rosakis, Phys. Rev. Lett. **106**, 155002 (2011).

[22] V. J. Anderson and H. N. W. Lekkerkerker, Nature **416**, 811 (2002).

[23] D. Frenkel, Science **314**, 768 (2006).

[24] H. Rothermel, T. Hagl, G. E. Morfill, M. H. Thoma, and H. M. Thomas, Phys. Rev. Lett. **89**, 175001 (2002).

[25] O. Arp, D. Block, M. Klindworth, and A. Piel, Phys. Plasmas **12**, 122102 (2005).

[26] L. Couëdel, M. Mikikian, L. Boufendi, and A. A. Samarian, Phys. Rev. E **74**, 026403 (2006).

[27] V. Land and W. J. Goedheer, New J. Phys. **8**, 8 (2006).

[28] H. W. Ellis, R. Y. Pai, E. W. McDaniel, E. A. Mason, and L. A. Viehland, Atom. Data Nucl. Data Tabl. **17**, 177 (1976).

[29] J. Neufeld and R. H. Ritchie, Phys. Rev. **98**, 1632 (1955).

[30] G. Joyce and D. Montgomery, Phys. Fluids **10**, 2017 (1967).

[31] D. Montgomery, G. Joyce, and R. Sugihara, Plasma Phys. **10**, 681 (1968).

[32] A. Melzer, V. A. Schweigert, and A. Piel, Phys. Rev. Lett. **83**, 3194 (1999).

[33] W. J. Miloch, J. Trulsen, and H. L. Pécseli, Phys. Rev. E **77**, 056408 (2008).

[34] A. V. Ivlev, J. Bartnick, M. Heinen, C.-R. Du, V. Nosenko, and H. Löwen, Phys. Rev. X **5**, 011035 (2015).

[35] M. Lampe, G. Joyce, G. Ganguli, and V. Gavrishchaka, Phys. Plasmas **7**, 3851 (2000).

[36] O. Ishihara and S. V. Vladimirov, Phys. Plasmas **4**, 69 (1997).

[37] S. Benkadda, V. N. Tsytovich, and S. V. Vladimirov, Phys. Rev. E **60**, 4708 (1999).

[38] R. Kompaneets, S. V. Vladimirov, A. V. Ivlev, and G. Morfill, New J. Phys. **10**, 063018 (2008).

[39] R. Kompaneetz and V. Tsytovich, Contrib. Plasma Phys. **45**, 130 (2005).

[40] M. Zeuner and J. Meichsner, Vacuum **46**, 151 (1995).

[41] A. V. Ivlev, S. K. Zhdanov, S. A. Khrapak, and G. E. Morfill, Phys. Rev. E **71**, 016405 (2005).

[42] Y. P. Raizer, *Gas Discharge Physics* (Springer-Verlag, Berlin, 1991).

[43] M. A. Lieberman and A. J. Lichtenberg, *Principles of Plasma Discharges and Materials Processing* (Wiley, New York, 1994).

[44] B. M. Smirnov, *Physics of Ionized Gases* (Wiley, New York, 2001), pp. 75–76.

[45] D. Else, R. Kompaneets, and S. V. Vladimirov, Phys. Plasmas **16**, 062106 (2009).

[46] M. Lampe, T. B. Röcker, G. Joyce, S. K. Zhdanov, A. V. Ivlev, and G. E. Morfill, Phys. Plasmas **19**, 113703 (2012).

[47] R. Kompaneets, G. E. Morfill, and A. V. Ivlev, Phys. Rev. Lett. **116**, 125001 (2016).

[48] S. A. Khrapak, B. A. Klumov, and G. E. Morfill, Phys. Rev. Lett. **100**, 225003 (2008).

[49] S. Khrapak and G. Morfill, Contrib. Plasma Phys. **49**, 148 (2009).

[50] M. Chaudhuri, S. A. Khrapak, R. Kompaneets, and G. E. Morfill, IEEE Trans. Plasma Sci. **38**, 818 (2010).

[51] M. Chaudhuri, A. V. Ivlev, S. A. Khrapak, H. M. Thomas, and G. E. Morfill, Soft Matter **7**, 1287 (2011).

[52] Y. Tyshetskiy and S. V. Vladimirov, Phys. Plasmas **17**, 103701 (2010).

[53] A. V. Filippov, A. G. Zagorodny, A. F. Pal', A. N. Starostin, and A. I. Momot, JETP Lett. **86**, 761 (2007).

[54] U. Konopka, G. E. Morfill, and L. Ratke, Phys. Rev. Lett. **84**, 891 (2000).

[55] R. Kompaneets, U. Konopka, A. V. Ivlev, V. Tsytovich, and G. Morfill, Phys. Plasmas **14**, 052108 (2007).

[56] R. Kompaneets, A. V. Ivlev, V. Nosenko, and G. E. Morfill, Phys. Rev. E **89**, 043108 (2014).

[57] R. Kompaneets, A. V. Ivlev, S. V. Vladimirov, and G. E. Morfill, Phys. Rev. E **85**, 026412 (2012).

[58] T. Peter, J. Plasma Phys. **44**, 269 (1990).